Functionalized Graphene-Based Quantum Dots: Promising Adsorbents for CO, NO_2, SO_2, and NH_3 Pollutant Gases

Rafael Ferreira de Menezes,[†] Fernando Pirani,[‡,¶] Cecilia Coletti,[§] Luiz Guilherme Machado de Macedo,[‖] and Ricardo Gargano*[,†]

[†]*Institute of Physics, University of Brasília, Campus Darcy Ribeiro, Brasília, DF, Brazil*

[‡]*Dipartimento di Chimica, Biologia e Biotecnologie, Universitá degli studi di Perugia, via Elce di Sotto 8, Perugia, Italy.*

[¶]*Dipartimento di Ingegneria Civile ed Ambientale, Università di Perugia. via Duranti 93, 06125 Perugia (Italy)*

[§]*Dipartimento di Farmacia, Università "G d'Annunzio" Chieti-Pescara, Via dei Vestini, Chieti, Italy*

[‖]*Universidade Federal de São João del Rei, Divinópolis, MG, Brazil*

E-mail: gargano@unb.br

Abstract

The development of more sensitive and accurate sensors is essential to monitor the levels of pollutant gases that are causing high damage to the biosphere. One of the most promising materials for such application is graphene, which, due to its extensive collection of properties, has shown itself capable of adsorbing gas molecules. Thus, the present work aims to investigate the adsorption of carbon monoxide (CO), nitrogen dioxide (NO_2), sulfur dioxide (SO_2), and ammonia (NH_3) on Graphene Quantum Dots

(GQD) through electronic structure and molecular dynamics calculations. The data suggest doping GQDs with boron, nitrogen, or aluminum can greatly improve their adsorbing capabilities. For both CO and NH_3, a functionalization with aluminum is the most effective, while the adsorption of SO_2 was not much affected by any of the doping designs. Notably, quantum dots doped with all three heteroatoms are extremely promising with respect to the application in NO_2 gas sensors. Thereby, the results indicate that accurate and resilient gas sensors based on doped GQDs may be a good substitute for the current sensors in the market.

Introduction

Currently, there is a great demand for more accurate and selective gas sensors due to the numerous applications in environmental monitoring, medicine, industry, and even in space missions.[1] The detection of pollutant gases such as carbon monoxide (CO), nitrogen dioxide (NO_2), sulfur dioxide (SO_2), and ammonia (NH_3) is extremely important due to the harmful effects these molecules have on ecosystems when present in high quantities due to anthropogenic activities.[2–4]

Graphene, due to its properties, sparked the interest of the scientific community for studies of nanosensors based on this extraordinary material. Experimental investigations pointed out that such systems can indeed be used as excellent gas sensors.[5] An exciting possibility is the use of graphene quantum dots (GQD) to adsorb small molecules. The generic term "quantum dot" refers to semiconductor particles with sizes up to a few nanometers. GQDs are a particular type of quantum dot obtained from nanometric fragments of graphene sheets.

The viability of a gas sensor is associated with the ability to adsorb the molecules of interest. Since graphene is the material with the highest surface-to-mass ratio, it maximizes the interaction with adsorbates making it extremely suitable for application in sensors. Nevertheless, a major limitation for its use as a gas sensor is the fact that pure graphene is chemically inert due to the strong covalent bond between sp^2 carbon atoms. However, studies indicate

that doping GQD with heteroatoms can have a profound impact on its properties.[6,7] In the perspective of gas sensing applications, boron, nitrogen, and aluminum are particularly promising heteroatoms to use for the functionalization of GQDs.[8]

Seeking to assert the effectiveness of a gas sensor, several crucial aspects ought to be investigated. Firstly, the electronic structure of the resulting complex must be studied. For instance, the potential energy curves (PECs) of the adsorption process provide important information on whether a given candidate is appropriate as far as its adsorbing properties are concerned. Another set of meaningful properties is the set of spectroscopic constants of the adsorbate-adsorbent complex, which reflect a signature of the adsorption mechanism. Finally, a decisive property that needs to be discussed is the lifetime of the complex. An adsorption process needs to be stable to be useful, in other words, large complex lifetimes mean that the physical or chemical process that binds the adsorbate to the adsorbent is effective. Moreover, it is essential to decompose the interaction energy in physically significant terms and consequently identify the most meaningful contributions to better comprehend the adsorption mechanism.

The literature is rich in works that seek to understand the process of adsorption on graphene, however, a study that evaluates all the above aspects simultaneously, especially the characterization of the interaction nature between the GQD (or the doped GQD) and the adsorbate is lacking. In addition, many papers study only one complex[9,10] and implement the usage of different software, which makes it difficult to compare the data. Even when more than one system is investigated, functionalization designs are usually not considered, and only interactions with pristine graphene sheets are studied.[11] As a result, the main contribution of the present work is to perform a broader investigation comparing, at the same level of theory, non-doped GQD and different functionalizations. The additional effort to shed light onto the nature of the interaction for all investigated GQDs allows to address the design of more effective graphene-based gas sensors.

Methodologies

Rovibrational spectroscopic properties

The rovibrational spectroscopic constants of each system were calculated employing two different and independent methodologies to ensure the coherence of the results. Firstly, by Dunham method,[12,13] and secondly, by the following equations:[14]

$$\begin{aligned}
\omega_e &= \frac{1}{24}\left[141\left(E_{1,0}-E_{0,0}\right)-93\left(E_{2,0}-E_{0,0}\right)+23\left(E_{3,0}-E_{1,0}\right)\right] \\
\omega_e x_e &= \frac{1}{4}\left[13\left(E_{1,0}-E_{0,0}\right)-11\left(E_{2,0}-E_{0,0}\right)+3\left(E_{3,0}-E_{1,0}\right)\right] \\
\omega_e y_e &= \frac{1}{6}\left[3\left(E_{1,0}-E_{0,0}\right)-3\left(E_{2,0}-E_{0,0}\right)+\left(E_{3,0}-E_{1,0}\right)\right] \\
\alpha_e &= \frac{1}{8}\left[-12\left(E_{1,1}-E_{0,1}\right)+4\left(E_{2,1}-E_{0,1}\right)+4\omega_e-23\omega_e y_e\right] \\
\gamma_e &= \frac{1}{4}\left[-2\left(E_{1,1}-E_{0,1}\right)+\left(E_{2,1}-E_{0,1}\right)+2\omega_e x_e-9\omega_e y_e\right]
\end{aligned} \tag{1}$$

where ω_e is the vibrational harmonic spectroscopic constant, $\omega_e x_e$ represents the first-order vibrational anharmonic constant, $\omega_e y_e$ is the second-order vibrational anharmonic constant, α_e and γ_e represent the rovibrational coupling constants (rotation-vibration interaction constants). In Eqs. 1, the $\mathrm{E}_{v,j}$ terms stand the rovibrational energies, where v and j are the vibrational and rotational quantum numbers, respectively. The $\mathrm{E}_{v,j}$ energies were calculated by solving the nuclear Schrödinger equation (NSE) through the DVR method.[15] To solve the NSE, within the Born-Oppenheimer approximation, it is necessary to know the analytical form of the potential energy curve that describes the interactions of the systems under study. In this work, the extended-Rydberg[16] analytical form was used, which has been shown to be an appropriate option to fit different molecular systems.[17–19] This analytical function is described according to the following equation:

$$V(R) = -D_e\left[1+\sum_{i=1}^{k} c_i (R-R_e)^i\right] e^{-c_1(R-R_e)} \tag{2}$$

where D_e is the dissociation energy, R_e represents the equilibrium distance and c_i are adjustable coefficients.

To determine the lifetime as a function of temperature for each complex within Slater theory,[20,21] the following equation was employed:

$$\tau(T) = \frac{1}{\omega_e} e^{\frac{D_e - E_{0,0}}{RT}} \tag{3}$$

where R represents the universal gas constant, T the temperature and $E_{0,0}$ the ground state rovibrational energy. As already mentioned, ω_e is the vibrational harmonic spectroscopic constant, and D_e is the dissociation energy.

Computational details

To obtain the PECs, the distance between the GQD and the molecule was systematically varied with a step of 0.1Å, performing a single point calculation in each iteration. After determining the equilibrium distance R_e, ten additional single points, with a step of 0.01Å, were calculated around the equilibrium value seeking to improve the accuracy of the results. As mentioned, the potential energy curves were fitted by the ten-coefficient extended-Rydberg function (Equation 2) using Powell method.[22]

The electronic energies were calculated employing the ωB97XD functional[23] with the 6-31G(d,p) basis set[24] as implemented in the Gaussian09 package.[25] Studies comparing this functional with other popular DFT functionals indicate that the ωB97XD functional delivers the best results when compared to experimental data for systems governed by van der Waals interactions.[26]

For the adsorbates CO, SO_2 and NH_3, the doping approach of the GQDs consisted of swapping the 22nd and the 44th carbons within the nanoflake (see Figure 1) with the three considered heteroatoms (B, N and Al). On the other hand, for the systems with NO_2, only the 44th carbon (C44) was swapped with the heteroatoms, so that the multiplicity

of all functionalized systems is equal to one. CO, NH_3, and SO_2 exhibit an electron lone pair mainly confined on the C, N, and S atom, respectively, while NO_2 is a free radical with an unpaired electron on N atom. In the present GQD, doping with B and Al atoms (with an electronic configuration ns^2np^1) generates a vacancy or defect of one electron on the nanostructure, while the doping with N ($2s^2 2p^3$) provides an excess of one electron. A number of different approaches was also tested, but none was as effective as the present one. The following notation was used to identify each system:

$$\text{Adsorbate} - \underbrace{\text{Adsorbent}}_{\text{GQD}} @nX \tag{4}$$

where n is the number heteroatoms and X is the dopant chemical symbol.

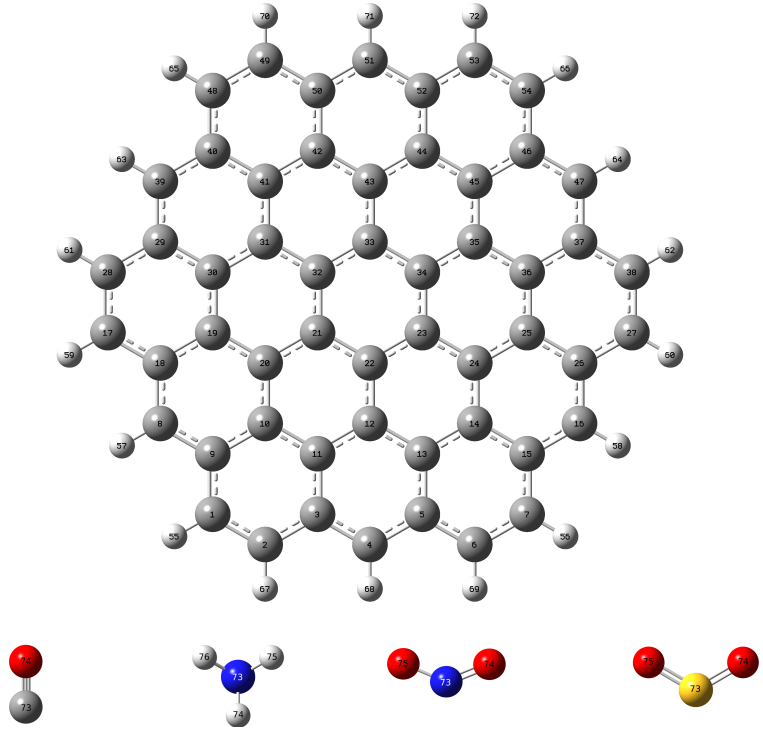

Figure 1: Schematic representation of a graphene quantum dot (composed by 54 carbons and 18 hydrogens) and the CO, NH_3, NO_2, and SO_2 adsorbates. The grey, red, white, blue, and yellow colors stand for carbon, oxygen, hydrogen, nitrogen, and sulfur, respectively.

The adsorbates can approach the quantum dot in many ways. For example, carbon monoxide can reach the GQD with a C-O bond that is parallel, perpendicular or any angle

in between, with respect to the quantum dot plane. In this work, the adsorbates approach the quantum dot through its 22th atom. Therefore, depending on the functionalization, the adsorbate will interact with a carbon, a boron, a nitrogen or an aluminum atom. Among the investigated geometries, the most stable ones were the following: the CO approaching the GQD perpendicularly with its carbon facing the quantum dot; the NH_3 approaching with its nitrogen facing the quantum dot; the NO_2 with with its nitrogen facing the quantum dot; and the SO_2 with its sulfur facing the quantum dot (see Figure 2). All these geometries see a lone pair (an unpaired electron in the case of NO_2) pointing to the GQD as the molecule approaches.

To better understand the electronic rearrangements occurring during the adsorption process of the pollutant molecules, the distribution of electron density in atoms and bonds between atoms were calculated by the Natural Bond Orbital Analysis (NBO)[27,28] implemented by the computational package Gaussian09, which contains the NBO program by F. Weinhold and coworkers.[29]

To describe the contributions for the interaction energies of each studied complex, the symmetry-adapted perturbation theory (SAPT)[30] was used, as implemented in the PSI4 computational package.[31,32] In the present case, SAPT0, i.e. the zero-th order truncation at the Hartree-Fock level, was employed because of the size of the system. Though the absolute values of the binding energies and of the different contributions to the interaction might not be very accurate, such a method still provides an indication of the energy partition in weakly bound complexes. Within this approach the interaction energy is decomposed into physically meaningful components, namely the electrostatic (E_{elst}), induction (E_{ind}), dispersion (E_{disp}), and exchange (E_{exch}) terms in the total electronic energy of the complexes under study.

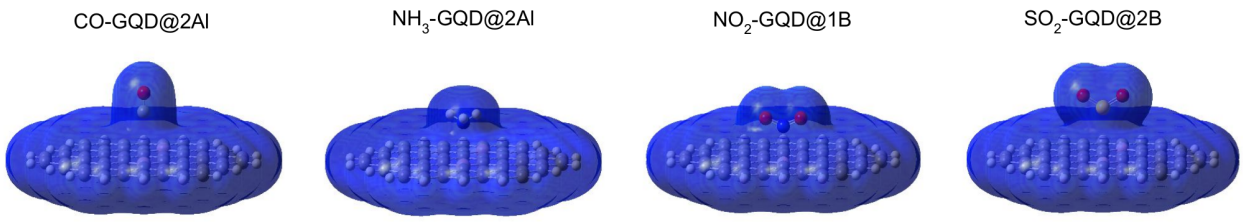

Figure 2: Electronic density of the most stable geometry for each adsorbate.

Results and Discussion

Potential energy curves

The electronic energies for a set of different internuclear distances, that range from the strong interaction region to the asymptotic region (weak interaction), were calculated at ωB97XD/6-31G(d,p) level for each investigated system and are shown in the Supplementary Material (Tables S1, S2, S3, and S4). These energies were adjusted to the analytical form given by Equation 2 and the fitted parameters (c_i) are presented in Table S5 of Supplementary Material. The dissociation energies D_e, the equilibrium distances R_e, and the reduced mass for each system are given in Table 1. For complexes involving non-functionalized graphene the binding energy D_e grows with the molecular polarizability of the incoming pollutant molecule, as expected for the van der Waals type of interaction, where most of the attraction is determined by the dispersion and induction components, as also shown by SAPT0 results (see below). This trend is confirmed by comparing the present results with those obtained for the adsorption of noble gases on graphene.[33] Since the polarizability of CO is close to that of Ar, and the polarizability of NH_3 is similar to that of Kr, one can expect the interactions GQD-CO and GQD-NH_3 to be comparable to those between graphene and the corresponding noble gas. Indeed the values obtained for such complexes (CO-GQD: 7.641 kJ/mol vs. Graphene-Ar: 9.378 kJ/mol;[33] NH_3-GQD: 12.175 kJ/mol vs. Graphene-Kr: 11.655 kJ/mol[33]) are in the right scale.

Table 1 and the PECs (Figure 3) clearly show that the considered doping schemes provide a more effective adsorption of the investigated molecules with respect to pristine graphene.

The systems with CO and NH_3 show a similar effect: the well depth is nearly doubled with boron doping, whereas doping with aluminum causes the strongest D_e increase, more than a factor 3 for NH_3. In the case of SO_2 the strength of adsorption upon doping is only slightly increased for all cases. The most striking enhancement is achieved for the NO_2 molecule, whose adsorption on doped GQDs becomes in all cases more than one order of magnitude more effective than in pristine graphene, with boron and aluminum again giving the strongest interaction. These results together with the D_e values suggest that the binding driving force in doped GDQs is not exclusively of van der Waals type, rather a covalent character of the interaction emerges, particularly when the NO_2 molecule, presenting an unpaired electron which can couple with the electron vacancy/excess of the dopant heteroatom, is at play. In all cases doping with nitrogen gives the less effective binding among functionalized GQDs: an excess electronic charge is less effective for the binding with the lone pair than electron vacancy.

All the above indications are sustained by the NBO and SAPT0 results presented in the following Section.

Spectroscopic properties

Using the fitted PECs for each system, the rovibrational energies were calculated (Tables S6, S7, S8, and S9 of Supplementary Material). The data reveal that the system NO_2-GQD@1B has the highest number of energy levels with 221, representing a gain of 183 energy levels in comparison with the non-functionalized system. On the other hand, the system NH_3-GQD has the lowest number of energy levels with 17. The highest number of energy levels for each adsorbate was obtained by a functionalization with either boron or aluminum, implying that those are the most auspicious dopants, especially for NO_2.

The spectroscopic constants of each system are presented in Table 3. Comparing the nu-

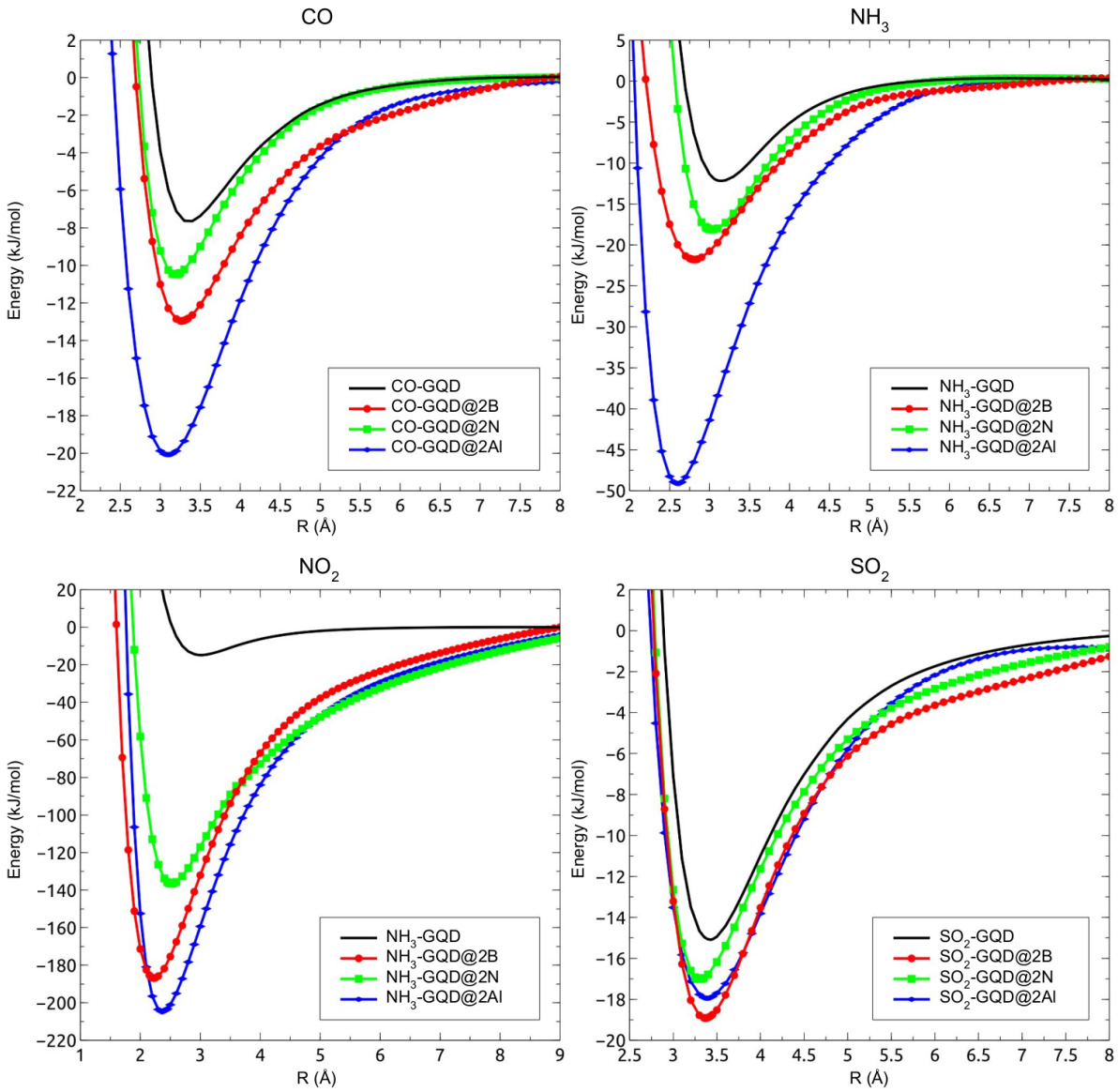

Figure 3: Potential energy curves for the interaction of the investigated pollutant molecules with differently doped GQD as a function of the distance R between the attacking atom of the incoming molecule (carbon for CO, nitrogen for NO_2 and NH_3, and sulfur for SO_2) and atom 22 in the GQD.

merical values obtained by both methods, one can verify that they are in excellent agreement, thus suggesting that the employed procedure is reliable. The lifetime of the systems was calculated within the Slater theory (Equation 3) and indicates that functionalization greatly improves the stability of the systems (see Table 2), a further indication of the potentiality of doped GQDs as effective gas sensing materials.

Table 1: Equilibrium distance R_e (Å), dissociation energies D_e (kJ/mol), calculated at ωB97XD/6-31G(d,p) level, and reduced mass μ (a.u.) of all studied systems.

Complex	R_e (Å)	D_e (kJ/mol)	μ (a.u)
CO-GQD	3.40	7.64	48999.9678
CO-GQD@2B	3.26	12.95	48992.8335
CO-GQD@2N	3.20	10.48	49011.7306
CO-GQD@2Al	3.11	20.07	49085.0247
NH_3-GQD	3.15	12.18	30271.4659
NH_3-GQD@2B	2.81	21.79	30268.7429
NH_3-GQD@2N	3.03	18.12	30275.9549
NH_3-GQD@2Al	2.60	49.12	30303.9071
NO_2-GQD	3.01	14.84	78448.7861
NO_2-GQD@1B	2.23	186.86	78439.6590
NO_2-GQD@1N	2.52	136.49	78463.9056
NO_2-GQD@1Al	2.36	204.76	78560.1536
SO_2-GQD	3.43	15.08	106534.6981
SO_2-GQD@2B	3.37	18.91	106500.9797
SO_2-GQD@2N	3.30	17.01	106590.3176
SO_2-GQD@2Al	3.39	17.95	106937.5883

Table 2: Lifetime (in seconds) as a function of the temperature calculated within the Slater theory.

Complex	Lifetime (s)			
	200 K	300 K	400 K	500 K
CO-GQD	4.8×10^{-11}	1.1×10^{-11}	5.3×10^{-12}	3.4×10^{-12}
CO-GQD@2B	9.7×10^{-10}	7.8×10^{-11}	2.2×10^{-11}	1.0×10^{-11}
CO-GQD@2N	2.0×10^{-10}	2.7×10^{-11}	9.8×10^{-12}	5.4×10^{-12}
CO-GQD@2Al	6.7×10^{-8}	1.3×10^{-9}	1.8×10^{-10}	5.5×10^{-11}
NH_3-GQD	3.5×10^{-10}	3.5×10^{-11}	1.1×10^{-11}	5.4×10^{-12}
NH_3-GQD@2B	1.0×10^{-7}	1.5×10^{-9}	1.8×10^{-10}	5.1×10^{-11}
NH_3-GQD@2N	9.9×10^{-9}	3.0×10^{-10}	5.3×10^{-11}	1.9×10^{-11}
NH_3-GQD@2Al	7.8×10^{-1}	5.0×10^{-5}	4.0×10^{-7}	2.2×10^{-8}
NO_2-GQD	3.0×10^{-9}	1.7×10^{-10}	4.0×10^{-11}	1.7×10^{-11}
NO_2-GQD@1B	6.8×10^{35}	4.5×10^{19}	3.7×10^{11}	5.1×10^{6}
NO_2-GQD@1N	6.2×10^{22}	9.6×10^{10}	1.2×10^{5}	3.4×10
NO_2-GQD@1Al	6.0×10^{40}	1.1×10^{23}	1.5×10^{14}	7.2×10^{8}
SO_2-GQD	5.0×10^{-9}	2.6×10^{-10}	5.9×10^{-11}	2.4×10^{-11}
SO_2-GQD@2B	4.7×10^{-8}	1.1×10^{-9}	1.7×10^{-10}	5.7×10^{-11}
SO_2-GQD@2N	1.4×10^{-8}	5.1×10^{-10}	9.5×10^{-11}	3.5×10^{-11}
SO_2-GQD@2Al	3.2×10^{-8}	9.3×10^{-10}	1.6×10^{-10}	5.5×10^{-11}

Table 3: Spectroscopic constants (cm^{-1}) calculated for all systems.

Complex	Method	ω_e	$\omega_e x_e$	$\omega_e y_e$	α_e	γ_e
CO-GQD	Equation (1)	56.40	0.78	3.85×10^{-2}	8.45×10^{-4}	4.13×10^{-5}
	Dunham	56.40	0.78	3.86×10^{-2}	8.50×10^{-4}	3.79×10^{-5}
CO-GQD@2B	Equation (1)	65.69	1.16	2.01×10^{-3}	9.73×10^{-4}	1.62×10^{-5}
	Dunham	65.68	1.16	3.45×10^{-3}	9.73×10^{-4}	1.60×10^{-5}
CO-GQD@2N	Equation (1)	70.10	1.44	3.11×10^{-3}	1.20×10^{-3}	1.78×10^{-5}
	Dunham	70.10	1.44	3.93×10^{-3}	1.20×10^{-3}	1.64×10^{-5}
CO-GQD@2Al	Equation (1)	68.58	0.53	4.72×10^{-3}	5.99×10^{-4}	9.05×10^{-6}
	Dunham	68.57	0.53	4.64×10^{-3}	6.00×10^{-4}	8.75×10^{-6}
NH_3-GQD	Equation (1)	100.07	2.06	1.57×10^{-2}	2.07×10^{-3}	4.08×10^{-5}
	Dunham	100.07	2.07	1.35×10^{-2}	2.08×10^{-3}	3.46×10^{-5}
NH_3-GQD@2B	Equation (1)	106.75	1.53	1.08×10^{-2}	1.77×10^{-3}	4.88×10^{-5}
	Dunham	106.73	1.53	1.26×10^{-2}	1.77×10^{-3}	4.80×10^{-5}
NH_3-GQD@2N	Equation (1)	118.94	2.23	4.51×10^{-3}	2.09×10^{-3}	2.59×10^{-5}
	Dunham	118.92	2.23	5.66×10^{-3}	2.09×10^{-3}	2.42×10^{-5}
NH_3-GQD@2Al	Equation (1)	161.70	1.51	1.02×10^{-2}	1.85×10^{-3}	1.49×10^{-5}
	Dunham	161.69	1.51	1.02×10^{-2}	1.85×10^{-3}	1.41×10^{-5}
NO_2-GQD	Equation (1)	65.11	0.90	9.43×10^{-4}	5.86×10^{-4}	5.62×10^{-6}
	Dunham	65.10	0.90	1.18×10^{-3}	5.84×10^{-4}	5.40×10^{-6}
NO_2-GQD@1B	Equation (1)	168.83	0.60	5.02×10^{-4}	3.71×10^{-4}	2.67×10^{-7}
	Dunham	168.82	0.60	4.80×10^{-4}	3.73×10^{-4}	2.99×10^{-7}
NO_2GQD@1N	Equation (1)	143.52	0.74	6.07×10^{-4}	3.52×10^{-4}	1.60×10^{-6}
	Dunham	143.51	0.74	6.79×10^{-4}	3.49×10^{-4}	1.60×10^{-6}
NO_2-GQD@2Al	Equation (1)	177.42	0.67	1.04×10^{-3}	3.58×10^{-4}	1.45×10^{-7}
	Dunham	177.40	0.67	1.02×10^{-3}	3.59×10^{-4}	1.21×10^{-7}
SO_2-GQD	Equation (1)	48.53	0.48	3.66×10^{-4}	2.56×10^{-4}	1.16×10^{-6}
	Dunham	48.52	0.48	2.42×10^{-4}	2.57×10^{-4}	1.05×10^{-6}
SO_2-GQD@2B	Equation (1)	51.41	0.41	2.11×10^{-3}	2.11×10^{-4}	1.95×10^{-6}
	Dunham	51.41	0.41	2.01×10^{-3}	2.10×10^{-4}	1.81×10^{-6}
SO_2-GQD@2N	Equation (1)	53.29	0.69	5.58×10^{-4}	3.12×10^{-4}	2.54×10^{-6}
	Dunham	53.28	0.69	9.06×10^{-5}	3.12×10^{-4}	2.60×10^{-6}
SO_2-GQD@2Al	Equation (1)	42.90	0.23	1.23×10^{-3}	2.16×10^{-4}	3.88×10^{-7}
	Dunham	42.89	0.23	9.58×10^{-4}	2.17×10^{-4}	7.04×10^{-7}

Energy decomposition and charge displacement

The results obtained by SAPT0/cc-pVDZ (Table 4) can provide some useful indications on the nature of the interactions and its change when graphene is doped. Indeed, even if the absolute value of each contribution to energy decomposition might not be accurate enough, the relative magnitude of dispersion (E_{disp}), attractive electronic (E_{elst}) and induction (E_{ind})

terms to the overall binding energy help to shed some light onto the nature of the adsorption process. The values reported in the table correspond to the minimum geometry for each investigated system.

For all systems involving pure GQD, the dispersion term E_{disp} dominates, exposing the non-covalent character of the interactions. However, functionalizations with boron and aluminum seem to diminish the relative influence of the dispersion term and to increase the relative contributions of other attractive contributions, that is electrostatic and induction terms. In the systems NH_3-GQD@2B, NH_3-GQD@2Al, and NO_2-GQD@1B, the enhancement is so large to dominate the global attraction. This, as anticipated, can be interpreted as an indication of a partial covalent kind of interaction, which at this level the SAPT method cannot fully catch.

Table 4: SAPT0/cc-pVDZ percentages of each contribution to the interaction energies determining the global stabilization effect at the equilibrium distance. E_{elst}, E_{ind}, and E_{disp} refer to electrostatic, induction, and dispersion attractive components, respectively.

Systems	$\%E_{elst}$	$\%E_{ind}$	$\%E_{disp}$
CO-GQD	23.2	5.0	71.8
CO-GQD@2B	30.4	7.6	62.0
CO-GQD@2N	28.6	4.5	66.9
CO-GQD@2Al	42.2	11.6	46.2
NH_3-GQD	22.3	18.9	58.8
NH_3-GQD@2B	40.7	21.5	37.8
NH_3-GQD@2N	36.0	14.5	49.5
NH_3-GQD@2Al	57.5	19.6	22.9
NO_2-GQD	26.4	10.4	63.2
NO_2-GQD@1B	42.1	17.1	40.8
NO_2-GQD@1N	27.2	35.1	37.7
NO_2-GQD@1Al	30.2	42.1	27.7
SO_2-GQD	33.3	9.6	57.1
SO_2-GQD@2B	35.9	10.6	53.5
SO_2-GQD@2N	27.3	10.5	62.2
SO_2-GQD@2Al	32.3	13.1	54.6

To deepen this aspect we performed a NBO analysis to evaluate the charge displacement between the adsorbates (CO, NH_3, NO_2, SO_2) and the adsorbent. Note that this kind of investigation cannot be performed within the SAPT approach, where charge transfer effects

are spread onto the various energy contributions. The results of NBO population analysis, i.e. the electron donor and acceptor orbitals, together with the second-order perturbation energies (E^2), whose value is connected to the magnitude of the charge delocalization, are reported in Table 5.

Table 5: Main NBO donor-acceptor analysis between filled and empty orbitals calculated at the ωB97XD/6-31G(d,p) level of theory. LP (LP*), BD (BD*) and RY* indicate 1-center valence lone pairs (empty orbital), 2-center bond (antibond) orbitals, and 1-center Rydberg orbitals, respectively. E^2 stands for second-order perturbation energies and indicates the stabililzation upon charge delocalization.

Complex	Donor	Acceptor	E^2(kJ/mol)
CO-GQD	BD C73 - O74	RY* C22	0.50
CO-GQD@2B	LP C73	LP* B22	14.36
CO-GQD@2N	LP C73	BD* N22 - C23	0.29
CO-GQD@2Al	LP C73	LP* Al22	56.87
NH_3-GQD	LP N73	BD* C21 - C22	1.29
NH_3-GQD@2B	LP N73	LP* B22	48.34
NH_3-GQD@2N	LP N73	RY* N22	0.79
NH_3-GQD@2Al	LP N73	LP* Al22	98.32
NO_2-GQD	BD C21 - C22	LP* N73	18.88
NO_2-GQD@1B	BD* C11 - C12	BD* B22 - N73	428.48
NO_2-GQD@1N	LP O75	BD* C21 - N22	11.79
NO_2-GQD@1Al	LP N73	LP* Al22	135.34
SO_2-GQD	BD C11 - C12	LP* S73	4.88
SO_2-GQD@2B	LP S73	LP* B22	13.34
SO_2-GQD@2N	LP S73	RY* N22	0.26
SO_2-GQD@2Al	LP S73	LP* Al22	37.28

In the case of the non-doped GQD, for all pollutant molecules but NO_2, there is only a negligible charge transfer, either from the adsorbant lone pair to graphene (CO and NH_3) or viceversa from graphene to the absorbant (SO_2 and NO_2, in the latter case, due to the presence of the unpaired electron, charge transfer is more sensitive).

Doping with boron and aluminum strongly enhances the displacement of the lone pair of CO, NH_3 and SO_2 towards the electron vacant heteroatom atom, again indicating a partial covalent character of the adsorption process. The charge delocalization is more marked in the case of aluminum. For NO_2 the above behavior is much more striking because of the coupling

between the unpaired electron of the dopant and of the incoming gas molecule. The strength of the interaction between the nitrogen dioxide and the quantum dot doped with boron is so high, that a 2-center covalent antibond orbital is formed between the nitrogen from NO_2 and the boron used in the functionalization (BD* B22-N73). This antibond receives charge from the 2-center antibond C11-C12.

On the other hand, doping with nitrogen, providing an extra electron with respect to pristine graphene, diminishes the acceptor nature of the GQD in the interaction, and the charge displacement is more limited for all the investigated gas molecules.

In summary, the important charge transfer contribution (a basic chemical interaction component) remarkably occurring in GQD doped with Al and B and for NO_2 and NH_3 interacting molecules, generates relevant additional stabilization effects. Additionally, the NO_2 and NH_3 molecules exhibit the lowest values of the ionization potential (940.7 kJ/mol and 979.3 kJ/mol, respectively).[34]

Moreover, the doping with N is almost ineffective, except for the free radical NO_2 (both N and NO_2 having an unpaired electron). These propensities, suggested by the chemical-physical properties of the interacting partners, are confirmed by the NBO analysis data.

Conclusions

The adsorbing capabilities of graphene quantum dots (GQDs) were investigated alongside with functionalizations schemes with heteroatoms (boron, nitrogen, and aluminum). In the present work, the focus is on electronic and dynamic properties of systems comprised of a GQD and the most common pollutant gas molecules (CO, NH_3, NO_2, and SO_2) whose monitoring of emissions is crucial to sustainable development.

The well depth of the potential energy curves, the related dissociation energy D_e and the increasing number of rovibrational energy levels upon functionalization point out that doping of GQDs can dramatically improve their absorbing capabilities. The extent of such

enhancement mostly depends on the electronic nature of the heteroatom. Spectroscopic constants were also calculated by two independent methodologies, which provided results in excellent agreement.

Indeed, the different magnitude of the adsorption energies can be explained by the analysis of the relative contributions to the total attraction and the electronic charge displacement between the incoming gas molecules and the GQD, which were carried out through SAPT0 and NBO approaches, respectively.

SAPT0 results show that the dispersion component dominates in the case of pristine GQDs. When doping with boron or aluminum is performed an electron vacancy arises: an empty orbital is available for the formation of an incipient coordination bond with the lone pair of NH_3, CO and SO_2. This covalent contribution to the absorption process very much enhances the interaction, particularly for CO and NH_3. In the case of NO_2, the presence of an unpaired electron, rather than of a lone pair, which can couple to the unpaired electron of doped GQDs makes the covalent nature of the interaction the driving force in the absorption as confirmed by the magnitude of D_e values more than one order of magnitude larger than those of non-doped GQDs.

Doping with nitrogen, on the other hand, present one electron excess, only moderately increasing the dissociation energy with respect to pristine graphene, and reducing the extent of the possibility of coordination bond when CO, NH_3 and SO_2 molecules are considered. However, the interaction with NO_2 molecule remains very strong, the pairing of two unpaired electrons stabilizing the electronic structure of both GQD@1N and NO_2.

In short, doping graphene quantum dots with heteroatoms is an effective way to enhance their interaction with pollutant gas molecules. For both carbon monoxide and ammonia, a functionalization with aluminum is the most effective, while the adsorption of sulfur dioxide was not very affected by any of the doping schemes. Particularly, doping quantum dots with either aluminum or boron, which create an electron vacancy, seems very promising for all the molecules investigated here. Note that a critical analysis of the interaction, highlighting the

most effective contributions to the adsorption process, can effectively guide the design of new and more efficient sensor devices. In this sense, a further step can be made by improving the description of the long range part of the potential, which is often basic for the orientation of the incoming molecule on the surface on the GQD, eventually determining the outcome of the molecular impact.

Acknowledgement

The authors thank the financial support from the Brazilian Research Councils: CAPES, CNPq and FAPDF.

Supporting Information Available

supporting_information.pdf - Electronic energies of the systems CO-GQD, CO-GQD@2B, CO-GQD@2N, and CO-GQD@2Al calculated at ωB97XD/6-31G(d,p) level, Electronic energies of the systems NH_3-GQD, NH_3-GQD@2B, NH_3-GQD@2N, and NH_3-GQD@2Al calculated at ωB97XD/6-31G(d,p) level, Electronic energies of the systems NO_2-GQD, NO_2-GQD@1B, NO_2-GQD@1N, and NO_2-GQD@1Al calculated at ωB97XD/6-31G(d,p) level, Electronic energies of the systems SO_2-GQD, SO_2-GQD@2B, SO_2-GQD@2N, and SO_2-GQD@2Al calculated at ωB97XD/6-31G(d,p) level, Fitting coefficients and root-mean-square deviation associated, Rovibrational energies of the systems CO-GQD, CO-GQD@2B, CO-GQD@2N, and CO-GQD@2Al, Rovibrational energies of the systems NH_3-GQD, NH_3-GQD@2B, NH_3-GQD@2N, and NH_3-GQD@2Al, Rovibrational energies of the systems NO_2-GQD, NO_2-GQD@1B, NO_2-GQD@1N, and NO_2-GQD@1Al, Rovibrational energies of the systems SO_2-GQD, SO_2-GQD@2B, SO_2-GQD@2N, and SO_2-GQD@2Al.

References

(1) Huang, B.; Li, Z.; Liu, Z.; Zhou, G.; Hao, S.; Wu, J.; Gu, B.-L.; Duan, W. Adsorption of Gas Molecules on Graphene Nanoribbons and its Implication for Nanoscale Molecule Sensor. *J. Phys. Chem. C* **2008**, *112*, 13442–13446.

(2) Krupa, S. Effects of Atmospheric Ammonia (NH_3) on Terrestrial Vegetation: a Review. *Environ. Pollut.* **2003**, *124*, 179–221.

(3) Peel, J. L.; Tolbert, P. E.; Klein, M.; Metzger, K. B.; Flanders, W. D.; Todd, K.; Mulholland, J. A.; Ryan, P. B.; Frumkin, H. Ambient Air Pollution and Respiratory Emergency Department Visits. *Epidemiol.* **2005**, 164–174.

(4) Biggeri, A.; Bellini, P.; Terracini, B. Meta-Analysis of the Italian Studies on Short-Term Effects of Air Pollution–MISA 1996-2002. *Epidemiol. prev.* **2004**, *28*, 4–100.

(5) Fowler, J. D.; Allen, M. J.; Tung, V. C.; Yang, Y.; Kaner, R. B.; Weiller, B. H. Practical Chemical Sensors from Chemically Derived Graphene. *ACS nano* **2009**, *3*, 301–306.

(6) Liu, H.; Liu, Y.; Zhu, D. Chemical Doping of Graphene. *J. Mater. Chem.* **2011**, *21*, 3335–3345.

(7) Zhang, Y.-H.; Chen, Y.-B.; Zhou, K.-G.; Liu, C.-H.; Zeng, J.; Zhang, H.-L.; Peng, Y. Improving Gas Sensing Properties of Graphene by Introducing Dopants and Defects: a First-Principles Study. *Nanotechnol.* **2009**, *20*, 185504.

(8) Dai, J.; Yuan, J.; Giannozzi, P. Gas Adsorption on Graphene Doped with B, N, Al, and S: A Theoretical Study. *Appl. Phys. Lett.* **2009**, *95*, 232105.

(9) Wanno, B.; Tabtimsai, C. A DFT Investigation of CO Adsorption on VIIIB Transition Metal-Doped Graphene Sheets. *Superlattices Microstruct.* **2014**, *67*, 110–117.

(10) Wehling, T.; Novoselov, K.; Morozov, S.; Vdovin, E.; Katsnelson, M.; Geim, A.; Lichtenstein, A. Molecular Doping of Graphene. *Nano Lett.* **2008**, *8*, 173–177.

(11) Lin, X.; Ni, J.; Fang, C. Adsorption Capacity of H_2O, NH_3, CO, and NO_2 on the Pristine Graphene. *J. Appl. Phys* **2013**, *113*, 034306.

(12) Dunham, J. The Energy Levels of a Rotating Vibrator. *Phys. Rev.* **1932**, *41*, 721.

(13) Dunham, J. The Wentzel-Brillouin-Kramers Method of Solving the Wave Equation. *Phys. Rev.* **1932**, *41*, 713.

(14) da Cunha, W. F.; de Oliveira, R. M.; Roncaratti, L. F.; Martins, J. B.; e Silva, G. M.; Gargano, R. Rovibrational Energies and Spectroscopic Constants for H_2O-Ng Complexes. *J. Mol. Model.* **2014**, *20*, 1–6.

(15) Prudente, F.; Costa, L.; Neto, J. S. Discrete Variable Representation and Negative Imaginary Potential to Study Metastable States and Photodissociation Processes. Application to Diatomic and Triatomic Molecules. *Comput. Theor. Chem.* **1997**, *394*, 169–180.

(16) Rydberg, R. Graphische Darstellung Einiger Bandenspektroskopischer Ergebnisse. *Z. Phys.* **1932**, *73*, 376–385.

(17) Vila, H. V. R.; Leal, L. A.; Fonseca, A.; Gargano, R. Calculation of the H_2^+ Rovibrational Energies and Spectroscopic Constants in the $2p\pi$, $3d\sigma$, $4d\sigma$, $4f\pi$, $4f\sigma$, $5g\sigma$, and $6i\sigma$ Electronic States. *Int. J. Quantum Chem.* **2012**, *112*, 829–833.

(18) Paura, E. N. C.; da Cunha, W. F.; de Oliveira Neto, P. H.; e Silva, G. M.; Martins, J. B.; Gargano, R. Vibrational and Electronic Structure Analysis of a Carbon Dioxide Interaction with Functionalized Single-Walled Carbon Nanotubes. *J. Phys. Chem. A* **2013**, *117*, 2854–2861.

(19) de Oliveira Neto, P. H.; Rodrigues, J. P.; de Sousa, L. E.; Gargano, R.; da Cunha, W. F. CO_2 Adsorption in Nitrogen-Doped Single-Layered Graphene Quantum Dots: a Spectroscopic Investigation. *J. Mol. Model.* **2019**, *25*, 1–5.

(20) Slater, J. C. The Theory of Complex Spectra. *Phys. Rev.* **1929**, *34*, 1293.

(21) de Menezes, R. F.; de Macedo, L. G. M.; Martins, J. B. L.; Pirani, F.; Gargano, R. Investigation of Strength and Nature of the Weak Intermolecular Bond in NH_2 Radical-Noble Gas Atom Adducts and Evaluation of Their Basic Spectroscopic Features. *Chem. Phys. Lett.* **2021**, *769*, 138386.

(22) Powell, M. A Method for Minimizing a Sum of Squares of Non-Linear Functions Without Calculating Derivatives. *Comput. J.* **1965**, *7*, 303–307.

(23) Chai, J.-D.; Head-Gordon, M. Long-Range Corrected Hybrid Density Functionals with Damped Atom–Atom Dispersion Corrections. *Phys. Chem. Chem. Phys.* **2008**, *10*, 6615–6620.

(24) Hehre, W. J.; Ditchfield, R.; Pople, J. A. Self—Consistent Molecular Orbital Methods. XII. Further Extensions of Gaussian—Type Basis Sets for Use in Molecular Orbital Studies of Organic Molecules. *J. Chem. Phys.* **1972**, *56*, 2257–2261.

(25) Frisch, M.; Trucks, G.; Schlegel, H. B.; Scuseria, G. E.; Robb, M. A.; Cheeseman, J. R.; Scalmani, G.; Barone, V.; Mennucci, B.; Petersson, G., et al. Gaussian 09, Revision d. 01, Gaussian. *Inc., Wallingford CT* **2009**, *201*.

(26) Minenkov, Y.; Singstad, Å.; Occhipinti, G.; Jensen, V. R. The Accuracy of DFT-Optimized Geometries of Functional Transition Metal Compounds: a Validation Study of Catalysts for Olefin Metathesis and Other Reactions in the Homogeneous Phase. *Dalton Trans.* **2012**, *41*, 5526–5541.

(27) Reed, A. E.; Weinstock, R. B.; Weinhold, F. Natural Population Analysis. *J. Chem. Phys.* **1985**, *83*, 735–746.

(28) Weinhold, F. Natural Bond Orbital Analysis: a Critical Overview of Relationships to Alternative Bonding Perspectives. *J. Comput. Chem.* **2012**, *33*, 2363–2379.

(29) Glendening, E. D.; Landis, C. R.; Weinhold, F. NBO 6.0: Natural Bond Orbital Analysis Program. *J. Comput. Chem.* **2013**, *34*, 1429–1437.

(30) Jeziorski, B.; Moszynski, R.; Szalewicz, K. Perturbation Theory Approach to Intermolecular Potential Energy Surfaces of Van Der Waals Complexes. *Chem. Rev.* **1994**, *94*, 1887–1930.

(31) Turney, J. M.; Simmonett, A. C.; Parrish, R. M.; Hohenstein, E. G.; Evangelista, F. A.; Fermann, J. T.; Mintz, B. J.; Burns, L. A.; Wilke, J. J.; Abrams, M. L., et al. Psi4: an Open-Source Ab Initio Electronic Structure Program. *Wiley Interdiscip. Rev. Comput. Mol. Sci.* **2012**, *2*, 556–565.

(32) Smith, D. G.; Burns, L. A.; Simmonett, A. C.; Parrish, R. M.; Schieber, M. C.; Galvelis, R.; Kraus, P.; Kruse, H.; Di Remigio, R.; Alenaizan, A., et al. PSI4 1.4: Open-Source Software for High-Throughput Quantum Chemistry. *J. Chem. Phys* **2020**, *152*, 184108.

(33) Bartolomei, M.; Carmona-Novillo, E.; Hernandez, M. I.; Campos-Martinez, J.; Pirani, F. Global Potentials for the Interaction Between Rare Gases and Graphene-Based Surfaces: an Atom–Bond Pairwise Additive Representation. *J. Phys. Chem. C* **2013**, *117*, 10512–10522.

(34) Radzig, A. A.; Smirnov, B. M. *Reference Data on Atoms, Molecules, and Ions*; Springer Science & Business Media, 2012; Vol. 31.